Influence of Non-Reciprocal Transceivers at 2.4 GHz in Adaptive MIMO-OFDM Systems

Markus Stefer*, Mark Petermann**, Martin Schneider*, Dirk Wübben**, Karl-Dirk Kammeyer**

*RF & Microwave Engineering Laboratory
University of Bremen, 28359 Bremen, Germany
Email:{markus.stefer, martin.schneider}@hf.uni-bremen.de

**Department of Communications Engineering
University of Bremen, 28359 Bremen, Germany
Email:{petermann, wuebben, kammeyer}@ant.uni-bremen.de

***Abstract*— In this paper, the impact of non-reciprocal transceivers is demonstrated by measurement results for different adaptive transmission strategies in a time division duplex MIMO-OFDM system. These strategies rely on the channel state information (CSI) at the transmitter, thus requiring either appropriate feedback or reciprocity of both communication links. The measurements were performed for point-to-point communication applying a bit and power loading algorithm. Furthermore, a point-to-multipoint scenario with zero forcing pre-equalization is considered. For both scenarios, equalization at the receiver is mandatory for imperfect CSI at the transmitter. To quantify the influence of the non-reciprocal transceivers on data transmission, the bit error rate determined by using the CSI obtained via the reverse link is compared with the bit error rate achieved by using perfectly fed back CSI of the forward link.**

I. Introduction

The demand for communication systems that are able to adapt to the given environment is increasing. Orthogonal frequency division multiplexing (OFDM) is the preferred transmission strategy due to its ability of adapting to frequency selective channels, e.g., utilizing water-filling based power allocation [1]. The need for feedback channels becomes obsolete if the channel state information (CSI) of the reverse link (RL) can be exploited for adaptive transmission strategies, such as beamforming and loading or even pre-equalization for the forward link (FL). Here, forward link can be seen analogously to downlink and reverse link in analogy to uplink. The usage of the aforementioned expresssions downlink and uplink is avoided because these terms are usually related with base station (BS) to mobile subscriber (MS) communication and vice versa.

To exploit adaptive transmission strategies, the CSI has to be known at the transmitter. Considering frequency division duplex (FDD) systems, this is realized by signaling the channel state information to the transmitter via a feedback channel. The reduction of spectral efficiency caused by the latter can be avoided by deploying time division duplex (TDD) [2]. In TDD systems, the reciprocity theorem can be utilized, which is valid for the physical multiple-input multiple-output (MIMO) channel between transmit and receive antennas [3]. However, the reciprocity theorem is violated for the corresponding digital baseband signals because of the different components used for assembling, e.g., the amplifiers and mixers, the digital-to-analog converter (DAC) and analog-to-digital converter (ADC) [4]. Moreover, the amplifiers and mixers introduce nonlinear effects, which add undesired frequency components [5]. DAC and ADC for example add differential and integral nonlinearities, the first describing the error regarding the quantization step width and the second denoting the error between ideal and actual output level [6].

In this contribution, the influence of the non-reciprocal transceivers on the bit error rate is investigated by setting up a TDD based measurement system. The latter is realized by the multiple antenna demonstrator MASI (**M**ultiple **A**ntenna **S**ystem for **I**SM-band transmission) in [7] additionally equipped with single-pole-double-throw (SPDT) switches connecting the corresponding transmit and receive chains with one antenna.

The paper is structured as follows. In Section II, the system model is introduced containing precoding [1] and pre-equalization [8] as well as the non-reciprocal transceivers [9], [10]. Subsequently, the measurement setup is explained in Section III and

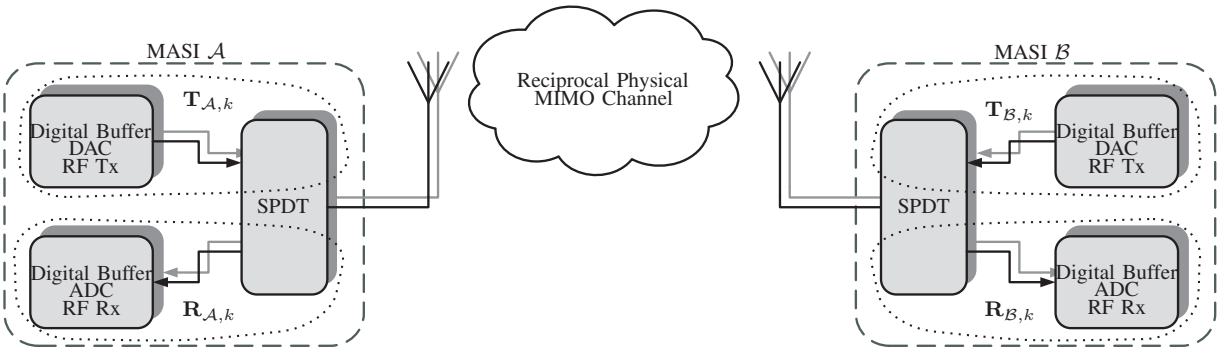

Fig. 1. Block diagram for modified MASI

the obtained results are presented in Section IV. Finally, concluding remarks are given in Section V.

II. System Model

The data transmission system consists of N_T transmit antennas and N_R receive antennas. OFDM based data transmission with N_{sc} subcarriers applies the inverse discrete fourier transform (IDFT) in combination with adding a cyclic prefix and transmitting the resulting signal. At the receiver, the cyclic prefix is discarded and the signal is converted back into the frequency domain by applying the discrete fourier transform (DFT). The system model used throughout this paper considers precoding or pre-equalization at the transmitter in general and linear equalization at the receiver. Receiver side equalization is realized by implementing the zero forcing (ZF) algorithm. Also, a power scaling factor β_k on each subcarrier $k = 0, \ldots, N_{sc} - 1$ is taken into account such that an increase in the transmit power is avoided. At the receiver, this power scaling factor is compensated. The data symbols $d_{t,k}$ on each antenna t and subcarrier k are taken from the odd integer grid of a M-QAM modulation scheme, $d_{k,t} \in \left\{ l + j \cdot m | l, m \in \left\{ \pm 1, \pm 3 \ldots, \pm\sqrt{M} - 1 \right\} \right\}$, scaled by $\sqrt{3/(2 \cdot (M-1))}$ to yield unit power. Hence, the estimated data symbols $\widetilde{\mathbf{d}}_k \in \mathbb{C}^{N_T}$ on each subcarrier k at the receiver can be expressed in frequency domain

$$\widetilde{\mathbf{d}}_k = \mathbf{H}^{\dagger}_{k,\text{eff}} \cdot \mathbf{H}^{\text{FL}}_k \cdot \mathbf{A}_{\text{pre},k} \cdot \mathbf{d}_k + \beta_k^{-1} \cdot \mathbf{n}_k \quad (1)$$

with white gaussian noise $\mathbf{n}_k$ with variance σ_n^2 and

- $\mathbf{H}^{\text{FL}}_k$ denoting the forward link channel matrix,
- $\mathbf{A}_{\text{pre},k}$ being the pre-equalization matrix,
- $\mathbf{H}_{k,\text{eff}} = \mathbf{H}^{\text{FL}}_k \cdot \mathbf{A}_{\text{pre},k}$ marking the effective channel

on each subcarrier k. Here, $(\bullet)^{\dagger}$ specifies the Moore-Penrose Pseudoinverse.

In general, the reciprocity theorem [3] only holds for the physical MIMO channel, meaning that $\mathbf{H}^{\text{FL}}_{k,\text{phys}} = \left(\mathbf{H}^{\text{RL}}_{k,\text{phys}}\right)^T$, $(\bullet)^T$ denoting the transpose. Including the receiver and transmitter chain RF devices of the MASI $\mathcal{A}$ and $\mathcal{B}$ shown in Fig. 1, $\mathbf{H}^{\text{FL}}_k$ and $\mathbf{H}^{\text{RL}}_k$ can be expressed as [9]

$$\mathbf{H}^{\text{FL}}_k = \mathbf{R}_{\mathcal{B},k} \cdot \mathbf{H}^{\text{FL}}_{k,\text{phys}} \cdot \mathbf{T}_{\mathcal{A},k} \text{ and} \quad (2a)$$

$$\mathbf{H}^{\text{RL}}_k = \mathbf{R}_{\mathcal{A},k} \cdot \mathbf{H}^{\text{RL}}_{k,\text{phys}} \cdot \mathbf{T}_{\mathcal{B},k}\,. \quad (2b)$$

The matrices $\mathbf{R}_{[\mathcal{A}/\mathcal{B}],k}$ and $\mathbf{T}_{[\mathcal{A}/\mathcal{B}],k}$ can be interpreted as error matrices on each subcarrier for the receiver and transmitter chains. The non-idealities stemming from the devices described in Section I are compressed into the aforementioned error matrices for each subcarrier. Rewriting (2b) and exploiting the reciprocity theorem for the physical channel, we get

$$\mathbf{H}^{\text{FL}}_k = \mathbf{R}_{\mathcal{B},k} \left(\mathbf{T}^{-1}_{\mathcal{B},k}\right)^T \left(\mathbf{H}^{\text{RL}}_k\right)^T \left(\mathbf{R}^{-1}_{\mathcal{A},k}\right)^T \mathbf{T}_{\mathcal{A},k}\,. \quad (3)$$

Hence, from (3) we can conclude that

$$\mathbf{H}^{\text{FL}}_k \neq \left(\mathbf{H}^{\text{RL}}_k\right)^T\,, \quad (4)$$

if $\mathbf{R}_{\mathcal{A},k} \neq \mathbf{T}_{\mathcal{A},k}$ and $\mathbf{R}_{\mathcal{B},k} \neq \mathbf{T}_{\mathcal{B},k}$. In case of non-reciprocal transceivers, which can be regarded as the general case, the reciprocity theorem is violated with respect to baseband processing.

Taking non-reciprocal transceivers into account, the following two scenarios were investigated:

1) point-to-point communication
2) point-to-multipoint communication

Point-to-point communication is also referred to as unicast channel (UC), and point-to-multipoint communication as broadcast channel (BC).

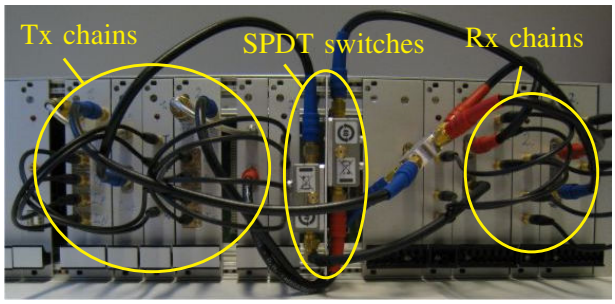

Fig. 2. MASI 19″ transceivers with SPDTs

For the UC case, the modulation scheme and the power scaling factor β_k on each subcarrier are obtained by applying a bit and power loading algorithm [11]. The latter relies on the singular value decomposition (SVD) of the channel matrix $\mathbf{H}_k^{\mathrm{FL}}$ or $\left(\mathbf{H}_k^{\mathrm{RL}}\right)^T$, respectively. Regarding the SVD, the channel matrices decompose into $\mathbf{H}_k^{\mathrm{FL}} = \mathbf{U}_k^{\mathrm{FL}}\,\mathbf{\Sigma}_k^{\mathrm{FL}}\,\left(\mathbf{V}_k^{\mathrm{FL}}\right)^H$ and $\left(\mathbf{H}_k^{\mathrm{RL}}\right)^T = \mathbf{U}_k^{\mathrm{RL}}\,\mathbf{\Sigma}_k^{\mathrm{RL}}\,\left(\mathbf{V}_k^{\mathrm{RL}}\right)^H$, $(\bullet)^H$ denoting the hermitian transpose. The precoding matrix becomes $\mathbf{A}_{\mathrm{pre},k} = \mathbf{V}_k^{[\mathrm{FL/RL}]}$. The effective channel assuming perfect knowledge of the FL CSI can be rewritten, such that

$$\begin{aligned}\mathbf{H}_{k,\mathrm{eff}} &= \mathbf{H}_k^{\mathrm{FL}}\,\mathbf{V}_k^{\mathrm{FL}} \\ &= \mathbf{U}_k^{\mathrm{FL}}\,\mathbf{\Sigma}_k^{\mathrm{FL}}\,\left(\mathbf{V}_k^{\mathrm{FL}}\right)^H\,\mathbf{V}_k^{\mathrm{FL}} \\ &= \mathbf{U}_k^{\mathrm{FL}}\,\mathbf{\Sigma}_k^{\mathrm{FL}}\,. \end{aligned} \tag{5}$$

Here, the pseudoinverse $\mathbf{H}_{k,\mathrm{eff}}^{\dagger}$ reduces to $\mathbf{H}_{k,\mathrm{eff}}^{\dagger} = \left(\mathbf{\Sigma}_k^{\mathrm{FL}}\right)^{-1}\left(\mathbf{U}_k^{\mathrm{FL}}\right)^H$, as was already proposed in [12]. Note, that the effective channel matrix in eq. (5) is only valid if channel estimation errors can be neglected. If only the RL CSI is known at the transmitter, the effective channel is described by

$$\begin{aligned}\mathbf{H}_{k,\mathrm{eff}} &= \mathbf{H}_k^{\mathrm{FL}}\,\mathbf{V}_k^{\mathrm{FL}} \\ &= \mathbf{U}_k^{\mathrm{FL}}\,\mathbf{\Sigma}_k^{\mathrm{FL}}\,\underbrace{\left(\mathbf{V}_k^{\mathrm{FL}}\right)^H\,\mathbf{V}_k^{\mathrm{RL}}}_{=\mathbf{V}_{k,\mathrm{int}}} \\ &= \mathbf{U}_k^{\mathrm{FL}}\,\mathbf{\Sigma}_k^{\mathrm{FL}}\,\mathbf{V}_{k,\mathrm{int}}\,. \end{aligned} \tag{6}$$

In this case, the pseudoinverse is equal to $\mathbf{H}_{k,\mathrm{eff}}^{\dagger} = \left(\mathbf{V}_{k,\mathrm{int}}\right)^{-1}\left(\mathbf{\Sigma}_k^{\mathrm{FL}}\right)^{-1}\left(\mathbf{U}_k^{\mathrm{FL}}\right)^H$. Therefore, by deploying an additional equalization at the receiver, we are able to mitigate the remaining interference denoted by $\mathbf{V}_{k,\mathrm{int}}$ [12].

For the BC case, the interference between the non-cooperative mobile subscribers has to be suppressed at the base station. Hence, applying the zero forcing algorithm at the transmitter results in the pre-equalization matrix $\mathbf{A}_{\mathrm{pre},k} = (\mathbf{H}_k^{[\mathrm{FL/RL}]})^{\dagger}$. Accordingly, the power scaling factor is equal to

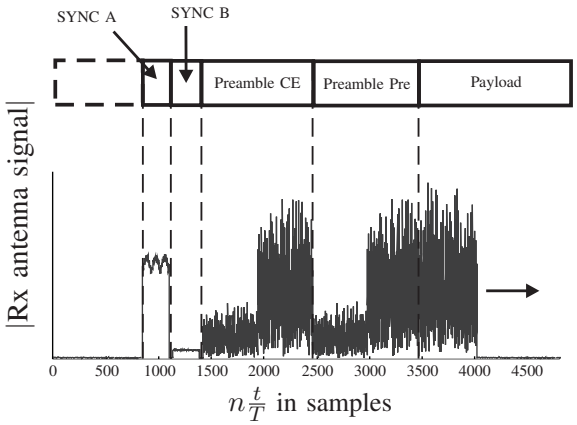

Fig. 3. Exemplary frame structure applied for MASI transmission

$\beta_k = \sqrt{N_T/||(\mathbf{H}_k^{[\mathrm{FL/RL}]})^{\dagger}||_F}$, where $\|\bullet\|_F$ describes the Frobenius norm [8]. If the forward link channel state information is available at the transmitter, the effective channel becomes the identity matrix $\mathbf{I}$.

$$\mathbf{H}_{k,\mathrm{eff}} = \mathbf{H}_k^{\mathrm{FL}}\,\left(\mathbf{H}_k^{\mathrm{FL}}\right)^{\dagger} = \mathbf{I} \tag{7}$$

Assuming eq. (7) holds, which is only the case in the absence of any channel estimation error, additional signal processing at the mobile subscribers can be neglected except the compensation for the factors β_k.

Exploiting the CSI of the reverse link leads to an effective channel matrix

$$\mathbf{H}_{k,\mathrm{eff}} = \mathbf{H}_k^{\mathrm{FL}}\,\left(\mathbf{H}_k^{\mathrm{RL}}\right)^{\dagger}\,. \tag{8}$$

In this case, eq. (1) has to be modified such that the pseudoinverse of the effective channel matrix $\mathbf{H}_{k,\mathrm{eff}}^{\dagger}$ is replaced by $\left(\mathbf{D}_{k,\mathrm{eff}}\right)^{-1}$, with

$$\mathbf{D}_{k,\mathrm{eff}} = \mathrm{dg}\{\mathbf{H}_{k,\mathrm{eff}}\} \tag{9}$$

and $\mathrm{dg}\{\bullet\}$ setting all off-diagonal entries of a matrix to zero.

III. Measurement Setup

The modified multiple antenna demonstrator MASI is used for the signal transmission, which is described in detail in [7]. In contrast to [13], each Tx/Rx chain, depicted in Fig. 2, is connected to a dipole antenna via a SPDT switch, resulting in a 2×2 transceiver system. The corresponding block diagram is shown in Fig. 1. The aforementioned SPDT switch is a pin-diode based switch classifed as P9402A manufactured by Agilent. The key features are an operating frequency ranging from 100 MHz to 8 GHz and an isolation of 80 dB. To minimize the effect of frequency synchronization errors, two

signal generators provide a sinusoidal signal with carrier frequency f_c for each MASI transceiver chain $\mathcal{A}$ and $\mathcal{B}$. The inevitable carrier frequency offset is compensated for by using the complex exponential denoted by "SYNC B" of the exemplary frame structure in Fig. 3. The sequence "SYNC A" of the frame structure shown in Fig. 3 allows for time synchronization using, e.g., a Zadoff-Chu or Barker sequence. The preambles "Preamble Pre" and "Preamble CE" are required for the channel estimation (CE) and are followed by the actual data, tagged with "Payload". The frames according to Fig. 3 are generated with Matlab and subsequently assigned to the internal memory of the demonstrator. The memory is read out and its content is transmitted periodically. The interested reader is referred to [7]. At this point, a line-of-sight (LOS) environment for the measurements is observed with both uniform linear arrays (ULA) broadside oriented at a distance of approximately $l \approx 3.175\,\mathrm{m}$. The channel is assumed to be time invariant for at least one TDD phase; starting with data transmission of one MS and ending with data reception of the same MS.

To evaluate the link equivalence, the precoding matrix $\mathbf{A}_{\text{pre},k}$ is computed based on

1) the estimated forward link channel matrix $\widehat{\mathbf{H}}_k^{\text{FL}}$ and
2) the estimated reverse link channel matrix $\left(\widehat{\mathbf{H}}_k^{\text{RL}}\right)^T$.

For the estimation of the channel matrices $\mathbf{H}_k^{[\text{FL/RL}]}$ a preamble of four OFDM symbols consisting of pre-equalized pilot symbols and symbols that are not pre-equalized is used. The pre-equalized pilot symbols, marked as "Preamble Pre" in Fig. 3, are taken for estimating the effective channel $\mathbf{H}_{k,\text{eff}}$, which is needed for the receiver-side post-processing [12]. Not pre-equalized pilot symbols, marked as "Preamble CE" in Fig. 3, give an estimation of the extended channel $\mathbf{H}_k^{[\text{FL/RL}]}$, which is required for the pre-equalization at the transmitter. Besides, the extended channel of the forward link $\mathbf{H}_k^{\text{FL}}$ is made available at the transmitter side via perfect feedback establishing an 802.11a ($5\,\mathrm{GHz}$) wireless LAN connection. Tab. I shows the settings for data transmission with the MASI demonstrator.

In the UC case, the point-to-point transmission between two MS with 2 antennas each is studied. Here, the two demonstrators MASI $\mathcal{A}$ and $\mathcal{B}$ are interpreted as two independent MS. In the BC case, the point-to-multipoint transmission between a BS with two antennas and two MS with one antenna each is evaluated. Regarding the demonstrator, the BS is realized by the MASI $\mathcal{A}$ and the two MS are realized by the MASI $\mathcal{B}$ (see Fig. 1). This is aquired by performing the digital signal processing separately for each receive and transmit signal of the transceiver chains $\mathcal{B}$. Due to the MASI hardware structure, the two transceivers of the MASI $\mathcal{B}$ are perfectly synchronized in time.

TABLE I
PARAMETERS FOR DATA TRANSMISSION.

Carrier Frequency	$f_c = 2.44\,\mathrm{GHz}$
Antenna Spacing	$d_{\text{ant}} = \lambda/2$
Subcarrier Spacing	$f_{\text{sc}} = 12.207\,\mathrm{kHz}$
Sampling Rate	$f_s = 50\,\mathrm{MHz}$
DFT Length	$N_{\text{sc}} = 512$
Guard Length	$N_g = 8$
Oversampling Factor	8
Modulation Scheme (no CC)	QPSK
Code Rate with 16QAM modulation	$R_c = 0.5$

IV. MEASUREMENT RESULTS

To obtain bit error rates (BER) versus receive symbol-to-noise ratios (Rx SNR), the Rx SNR is modeled by adding extra white Gaussian noise to the receive signal at the symbol rate. The corresponding noise variances of the different receive symbol-to-noise ratios are calculated and scaled depending on the measured receive symbol power. Fig. 4 compares the BER for different Rx SNR using $\widehat{\mathbf{H}}_k^{\text{FL}}$ and $(\widehat{\mathbf{H}}_k^{\text{RL}})^T$, respectively, for data transmission with and without channel coding (CC) in case of the unicast channel. For the measurements with CC a half-rate convolutional code with constraint length three is applied. In the uncoded case, the use of the FL CSI leads to an advantage of approximately $10\,\mathrm{dB}$ over the usage of the reverse link CSI at a BER of 10^{-3}. In contrast, this advantage decreases when applying channel coding, yielding a gap of approximately $2\,\mathrm{dB}$ at a BER of 10^{-3}. Overall, precoding the data based on $\widehat{\mathbf{H}}_k^{\text{FL}}$ and applying bit and power loading [11], outperforms the use of the estimated reverse link channel matrix as expected.

Fig. 5 depicts the BER vs. Rx SNR curves for the point-to-multipoint communication scenario. Without channel coding, the use of the FL CSI results in less errors compared to the usage of the RL CSI as well, namely approximately $3.5\,\mathrm{dB}$ at a BER of 10^{-3}. Similarly to the UC case, the difference declines to approximately $1\,\mathrm{dB}$ for applied channel coding with respect to the receive SNR at a BER of 10^{-3}. Hence, the exploitation of RL CSI is justified when using forward error correction although facing

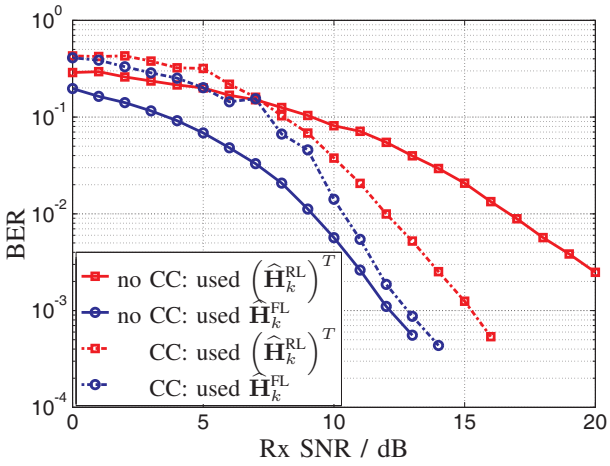

Fig. 4. Bit error rate for data transmission for the UC scenario.

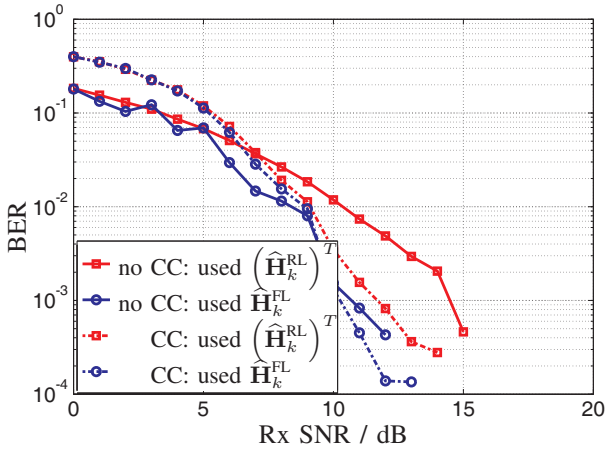

Fig. 5. Bit error rate for data transmission for the BC scenario.

the effects of non-reciprocal transceivers. This is also substantiated by the fact that additional loss due to quantization is expected when using FL CSI in feedback limited systems.

V. Conclusion

In this paper, measurement results for different pre-equalization techniques in combination with and without channel coding are presented. On one hand pre-equalization is based on the forward link channel state information; alternatively, channel state information is gained from the reverse link. Exploiting CSI obtained from the reverse link shows promising results, only when combining it with channel coding for both the UC and BC scenario. The non-reciprocal properties of the transceiver chains obviously decrease the system performance, which could exemplarily be shown with a multiple antenna demonstrator using off-the-shelf components. In the future, the influence of online calibration schemes as proposed in [9] would be interesting to determine. It is expected that applying calibration results in a lower BER, hence, letting the difference between forward link and reverse link based pre-equalization vanish [14]. This can be interpreted as forcing the extended channel to match the reciprocity theorem, i.e., equality holds in eq. (4).

References

[1] J. G. Proakis and M. Salehi, *Digital Communications*, McGraw-Hill, fifth edition, 2008.

[2] A. E. Ekpenyong and Y.-F. Huang, "Feedback Constraints for Adaptive Transmission," *IEEE Signal Processing Magazine*, vol. 24, no. 3, pp. 69–78, May 2007.

[3] C. Altman and K. Suchy, *Reciprocity, Spatial Mapping and Time Reversal in Electromagnetics*, vol. 9, Kluwer Academic Publishers, 1991.

[4] J. Liu, A. Bourdoux, J. Craninckx, B. Come, P. Wambacq, S. Donnay, and A. Barel, "Impact of Front-end Effects on the Performance of Downlink OFDM-MIMO Transmission," in *IEEE Radio and Wireless Conference (RAWCON)*, Sep 2004, pp. 159–162.

[5] D. M. Pozar, *Microwave Engineering*, John Wiley & Sons, 2nd edition, 1998.

[6] U. Tietze and Ch. Schenk, *Halbleiterschaltungstechnik*, Springer, 2002.

[7] J. Rinas, R. Seeger, L. Brötje, S. Vogeler, T. Haase, and K.-D. Kammeyer, "A Multiple-Antenna System for ISM-Band Transmission," *EURASIP Journal on Applied Signal Processing*, vol. 2004, no. 9, pp. 1407–1419, Aug 2004.

[8] C. Windpassinger, *Detection and Precoding for Multiple Input Multiple Output Channels*, Ph.D. thesis, University Erlangen-Nuremberg, Germany, 2004.

[9] M. Guillaud, *Transmission and Channel Modeling Techniques for Multiple-Antenna Communication Systems*, Ph.D. thesis, Ecole Nationale Supérieure des Télécommunications, France, 2005.

[10] W. Keusgen, *Antennenkonfigurationen und Kalibrierungskonzepte für die Realisierung reziproker Mehrantennensysteme*, Ph.D. thesis, RWTH Aachen, Germany, 2005.

[11] B. S. Krongold, K. Ramchandran, and D. L. Jones, "Computationally Efficient Optimal Power Allocation Algorithms for Multicarrier Communication Systems," *IEEE Transactions on Communications*, vol. 48, no. 1, pp. 23–27, Jan 2000.

[12] H. Busche, A. Vanaev, and H. Rohling, "SVD-based MIMO Precoding and Equalization Schemes for Realistic Channel Knowledge: Design Criteria and Performance Evaluation," *Wireless Personal Communications*, vol. 48, no. 3, pp. 347–359, 2009.

[13] R. Seeger, L. Brötje, and K.-D. Kammeyer, "A MIMO Hardware Demonstrator: Application of Space-Time Block Codes," in *IEEE Symposium on Signal Processing and Information Technology (ISSPIT 03)*, Darmstadt, Germany, Dec 2003.

[14] M. Petermann, D. Wübben, and K.-D. Kammeyer, "Calibration of Non-Reciprocal Transceivers for Linearly Pre-Equalized MU-MISO-OFDM Systems in TDD Mode," in *14th International OFDM-Workshop 2009 (InOWo 09)*, Hamburg, Germany, Sep 2009.